

A statistical reference-free damage identification for real-time monitoring of truss bridges using wavelet-based log likelihood ratios

Soon Gie Lee¹ and Gun Jin Yun^{*2}

¹Daewoo Shipbuilding and Marine Engineering Co. LTD., 656-714, Geoje, South Korea

²Department of Civil Engineering, The University of Akron, Akron, OH 44325-3905, USA

(Received September 11, 2011, Revised December 27, 2012, Accepted January 27, 2013)

Abstract. In this paper, a statistical reference-free real-time damage detection methodology is proposed for detecting joint and member damage of truss bridge structures. For the statistical damage sensitive index (DSI), wavelet packet decomposition (WPD) in conjunction with the log likelihood ratio was suggested. A sensitivity test for selecting a wavelet packet that is most sensitive to damage level was conducted and determination of the level of decomposition was also described. Advantages of the proposed method for applications to real-time health monitoring systems were demonstrated by using the log likelihood ratios instead of likelihood ratios. A laboratory truss bridge structure instrumented with accelerometers and a shaker was used for experimental verification tests of the proposed methodology. The statistical reference-free real-time damage detection algorithm was successfully implemented and verified by detecting three damage types frequently observed in truss bridge structures – such as loss of bolts, loosening of bolts at multiple locations, sectional loss of members – without reference signals from pristine structure. The DSI based on WPD and the log likelihood ratio showed consistent and reliable results under different damage scenarios.

Keywords: real-time monitoring; structural health monitoring (SHM); wavelet packet decomposition (WPD); likelihood; reference-free; truss bridge structure; damage identification

1. Introduction

Early damage detection in the civil infrastructure has been considered critical for achieving goals in the field of structural health monitoring (SHM). The recent collapse of the I-35 W bridge in Minneapolis highlights the importance of early damage detection in bridge structures for public safety. Nowadays, advances in sensors and information technology (IT) render the real-time SHM for civil infrastructure viable. In particular, developments of damage sensitive index (DSI) and real-time SHM system are critical factors for early damage detection in civil infrastructure. The real-time SHM system has been gaining attention, since it can raise an alarm about significant damaging events during operations, thereby providing more time for evacuation of users and timely maintenance of civil infrastructure. Therefore, there are apparent advantages of real-time

*Corresponding author, Associate Professor, E-mail: gy3@uakron.edu

monitoring of the structural health of civil infrastructure: it allows us to ensure both servicability and safety, and it prevents any catastrophic disaster.

There has been a vast amount of literature and reports on the online real-time SHM system for bridge structures. Nigbor and Diehl developed an online alerting of structural integrity and safety (OASIS) system that can remotely monitor two bridges in Thailand and Korea (Nigbor and Diehl 1997). Aktan *et al.* instrumented the Commodore Barry bridge in Philadelphia as a test bed with real-time environmental monitoring systems which can monitor the live loading, speed of wind and temperature at several locations of the bridge (Aktan *et al.* 2004). Masri *et al.* applied a web enabled real-time SHM system to Vincent Thomas Bridge in California (Masri *et al.* 2004). With increasing awareness of the importance of monitoring the structural health over the entire life cycle, it is a recent trend that built-in SHM systems are planned and designed before construction phases for long-term monitoring and maintenance of structures.

However, there have been difficulties in applications of the vibration-based real-time SHM system to damage detection and continuous condition assessment because of limitations in fast signal processing and inherent uncertainties due to environmental effects, including temperature and humidity. Most of vibration-based SHM and damage detection techniques have employed theoretical rationales, including the argument that changes in modal properties are directly related to changes in structural stiffness and damping. Damage detection techniques based on finite element model updating focus on the identification of changes in the parameters defined within numerical models. In case of large-scale structures, such model-based diagnosis methods are not adequate to real-time monitoring due to tremendous computational times. On the contrary, model-free methods are based on pattern recognitions of response signals from the structural system. As a real-time damage detection algorithm, a DSI based on coefficients of the autoregressive (AR) time series model was introduced by Nair *et al.* (2007) and an AR model-based damage detection algorithm was developed with Gaussian mixture model (GMM) of feature vector and tested with the ASCE benchmark structure. But this algorithm has limited usage for the linear stationary response signal. Jiang and Adeli developed multiple signal classification (MUSIC) and fuzzy wavelet neural network (WNN) with pseudospectrum method (Jiang and Adeli 2007). They used response signals from the 1:20 scaled 38-story concrete test model developed by Ni *et al.* (Ni *et al.* 2006). MUSIC and WNN tools can be used for the real-time SHM especially for the high rise building structures. (Jiang and Adeli 2007).

The wavelet transformation (WT) method is an effective tool for applications such as signal denoising, wave propagation based damage detection, signal compression and feature extraction. Due to the computational efficiency of the WT, it holds potentials for applications in real-time SHM and damage detection. According to the literature (Liew and Wang 1998), the wavelet based damage detection method has the advantage of simplicity in implementation, when compared to traditional eigenvalues analysis for detecting structural damage. Liew and Wang also pointed out the inaccuracy of eigenvalue analysis in higher-order modes caused by the limitation of mathematical and computation modeling, but they find that wavelet analysis does not have this problem. Moreover, wavelet analysis can reveal local information of non-stationary signals by zooming in at any interval of time and frequency. For these reasons, a variety of studies on SHM and damage detection have been conducted by applying the WT (Grabowska *et al.* 2008, Hu and Afzal 2006, Jiang and Mahadevan 2008, Jiang *et al.* 2007, Liew and Wang 1998, Ovanesova and Suarez 2004, Taha *et al.* 2006, Tsai *et al.* 2006, Wang and McFadden 1996) or WPD (Amiri and Asadi 2009, Chang and Sun 2005, Chendeb *et al.* 2006, Ding and Li 2007, Han *et al.* 2005, Jiang *et al.* 2007, Shinde and Hou 2005, Sun and Chang 2002, Sun and Chang 2007, Yen and Lin 2000,

Zhou *et al.* 2005) to different types of structures.

Most existing damage detection methods require signals from undamaged pristine structures to be compared with signals from damaged structures. Without signals from the original undamaged state, it is usually impossible to detect damage in structures. Therefore, a reference-free damage detection algorithm is introduced in this paper. The reference-free schemes do not depend on the response of previous healthy conditions. Kim and Sohn developed a reference-free crack detection methodology which does not require baseline data for crack detection for a plate-like structure with uniform thickness by examining measured Lamb wave signals (Kim and Sohn 2007). This methodology can reduce the false alarms caused by changing operational and environmental variations. In this paper, a statistical reference-free damage identification method was proposed for use in real-time SHM system. For this purpose, a WPD method was adopted in the proposed real-time SHM algorithm. The WPD decomposes original time domain signals into several frequency bands by the corresponding scales. The wavelet coefficients from a certain frequency range that are sensitive to the local damage can be selected for damage detection. Based on the selected wavelet coefficients, the log likelihood ratio is calculated to obtain the DSIs. In particular, the proposed real-time damage detection method is capable of detecting damage without response signals from healthy structures by comparing the sum of the log likelihood ratios of the wavelet coefficients between different sensor locations. The real-time reference-free damage detection system was implemented by using the National Instruments (NI) LabVIEW virtual instruments (VI) program in conjunction with the NI data acquisition (DAQ) system. A remote front panel was published on a remote collaboratory web-site by a web-publishing tool supported by the NI-LabVIEW. A laboratory structure that is a part of the remote collaboratory system (Yun 2010) was used for demonstration tests.

2. Statistical reference-free damage detection based on WPD

In the sequel, theoretical backgrounds and advantages of the WPD over the conventional WT will be revisited and the proposed reference-free damage sensitive feature will be introduced.

2.1 Wavelet packet decomposition

Compared to the Fourier transform, which uses simple harmonic functions (sine and cosine) as a basis, the wavelet transform allows for a wider choice of basis functions. This flexibility allows the wavelet transform to isolate changes in a signal that may be difficult to detect using other transform methods. This advantage of the wavelet transform is naturally inherited by wavelet-based measures of energy and entropy, and it leads to better damage identification (Yun *et al.* 2011). For this reason, wavelet transform methods such as continuous wavelet transform (CWT), discrete wavelet transform (DWT), and WPD have been widely used as signal analysis methods (Newland 1993). Wavelet transform and wavelet packets based damage detection is widely used in many vibration based SHM and damage detection applications (Chendeb *et al.* 2006, Han *et al.* 2005, Jiang and Mahadevan 2008, Sun and Chang 2007, Yen and Lin 2000). Wavelet transforms have advantages when the signal is non-stationary, since they describe signals in localized time and frequency domains. However, the DWT can hold poor frequency resolution in the higher frequency range and thus has limitations in analyzing signals that contain close high frequency components. The WPD is a technique to decompose signals repeatedly into successive

low and high frequency components up to the targeted frequency scale. Whereas the DWT decomposes only the approximations, the WPD decomposes both the approximations and details at a given scale of decomposition. Therefore the WPD is more flexible and has wider basis with higher resolutions for the analysis of signals than the DWT. The WPD also enables multi resolution damage detection, since it can localize multi-frequency bands in any time domain.

Wavelet packet $\Psi_{j,k}^i$ shown in Eq. (1) holds properties such as orthonormality and time-frequency localization inherited from wavelet functions (Coifman and Wickerhauser1992). The index i denotes the modulation; j and k represent the scale and translation parameters, respectively.

$$\Psi_{j,k}^i = 2^{j/2} \Psi^i(2^j t - k) \quad \Psi^1 - \text{Basis Function (Mother Wavelet)} \quad i = 1, 2, 3 \dots \quad (1)$$

The first wavelet function Ψ^1 is called a mother wavelet function; this satisfies the invertability and orthogonality. Wavelet analysis has a very wide choice of basis functions, such as Haar, Daubechies, Symlets, Coiflets, etc. In this paper, Daubechies2 (db2) was selected for the mother wavelet. Daubechies wavelet is a type of orthogonal wavelet. It has asymmetrical properties and possesses good compression. Detailed information about the Daubechies wavelet can be found in (Daubechies 1992). The wavelets Ψ^1 are obtained from the following recursive relationships as shown in Eqs. (2) and (3) (Sun and Chang 2002).

$$\Psi^{2^{i-1}}(t) = (2)^{1/2} \sum_{k=-\infty}^{\infty} l(k) \Psi^i(2t - k) \quad (2)$$

$$\Psi^{2^i}(t) = (2)^{1/2} \sum_{k=-\infty}^{\infty} h(k) \Psi^i(2t - k) \quad (3)$$

In these equations, $h(k)$ and $l(k)$ are the high pass filter and low pass filter. The schematic structure of the decomposed wavelet packet tree of an original time domain signal $S(t)$ was shown in the Fig. 1. The schematic diagram shows wavelet packet transforms up to the third frequency scale.

In each scale, the original signals are decomposed through the low pass filter L and high pass filter H. Unlike the wavelet transform, the WPD allows details ($D_{j,k}$: $j=j$ th scale and $k=1, \dots, 2j-2$) to be filtered by the high pass filter. It thus provides higher resolution in the higher frequency band. A recursive relationship between j th and $(j+1)$ th scale decompositions is satisfied as

$$S_j^i(t) = S_{j+1}^{2^{i-1}}(t) + S_{j+1}^{2^i}(t) \quad (4)$$

The filtered time-domain signals in Eq. (4) can be written as

$$S_{j+1}^{2^{i-1}}(t) = LS_j^i(t) \quad \text{and} \quad S_{j+1}^{2^i}(t) = HS_j^i(t) \quad (5)$$

where L and H are filtering-decimation operators that are related with discrete filters $l(k)$ and $h(k)$ as

$$L\{\cdot\} = \sum_{k=-\infty}^{\infty} l(k - 2t) \quad \text{and} \quad H\{\cdot\} = \sum_{k=-\infty}^{\infty} h(k - 2t) \quad (6)$$

After j th scale decomposition, the original time-domain signals $S(t)$ is expressed as

$$S(t) = \sum_{i=1}^{2^j} S_j^i(t) \tag{7}$$

Then the wavelet packet time-domain signals $S_j^i(t)$ are expressed by a linear combination of wavelet packet function $\Psi_{j,k}^i$ as follows(Sun and Chang 2002)

$$S_j^i(t) = \sum_{k=-\infty}^{\infty} C_{j,k}^i \Psi_{j,k}^i(t) \tag{8}$$

Under the orthogonality property of wavelet packet function (i.e., $\Psi_{j,k}^m \Psi_{j,k}^n = \delta_{mn}$ where δ_{mn} is the Kronecker delta), the wavelet packet coefficients can be obtained as

$$C_{j,k}^i = \int_{-\infty}^{+\infty} S(t) \Psi_{j,k}^i(t) dt \tag{9}$$

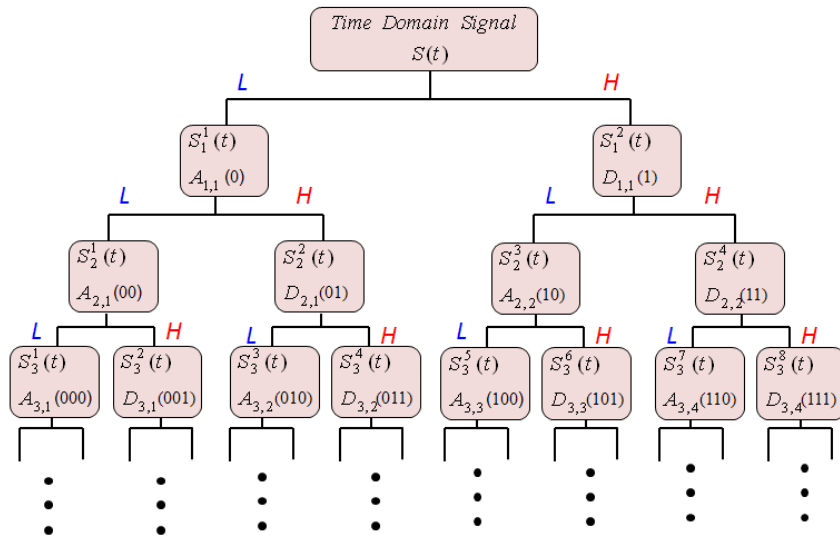


Fig. 1 Schematic structure of the WPD

Due to the time-frequency multi-resolution property of the wavelet packet transform, adequate selection of wavelet packets is critical for successful damage detection. Frequency bands of the chosen wavelet packets should include fundamental natural frequencies of the structure since damage changes the natural frequencies. Selection of the mother wavelet and the number of scales of the wavelet transform are also important for successful detection of damage. In this analysis, the Daubechies2 (db2) mother wavelet was selected and sixth scale wavelet packets were tested considering the frequency band of the wavelet packets. Sun and Chang reported the importance of having sufficient magnitudes of wavelet packet coefficients, enough to reveal trivial changes in

vibration signals subjected to noise and errors in real-life measurements (Sun and Chang 2002). As in the wavelet transforms (Yun *et al.* 2011), the level of decompositions of WPD is also one of the most important factors in order to detect local damage in structures (Sun and Chang 2002). The required level of decompositions can vary depending on the level of damage and loading conditions. Therefore, it is desirable to perform sensitivity analysis based on wavelet energy ratio (Yun *et al.* 2011) or energies of components (Sun and Chang 2002) for selecting proper wavelet packets. In this paper, a sensitivity analysis was performed based on log likelihood ratios with a gradual increase of damage level.

For convenience in selecting wavelet packets, a path notation in terms of binary codes was used as shown in the Fig. 1. The path notation is used in the NI-LabVIEW VI program to choose the packet of specific frequency band that is sensitive to the damage, since damage changes the energy and frequency contents in the response acceleration signals. Damage sensitive features are defined as log likelihood ratios of different sets of the packets corresponding to the frequency bands of our interest.

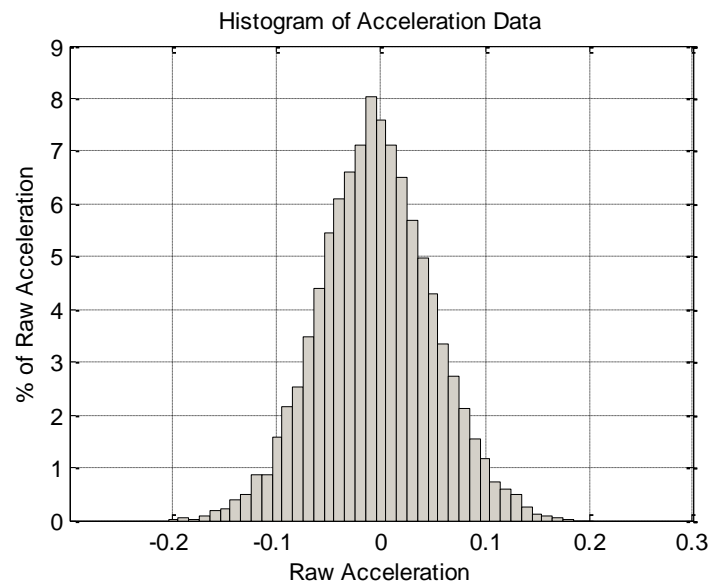


Fig. 2 Histogram of raw acceleration data measured from a laboratory structure subjected to broad-band white noise (500 mV amplitude)

2.2 Log likelihood ratio for damage identification

Likelihood function was introduced in mathematical statistics by Fisher in 1922 (Aldrich 1997). The likelihood function is frequently used in the likelihood ratio test for the purpose of quantifying the fitness between the probability distributions or in the maximum likelihood estimate of probabilistic parameters that maximize the likelihood of obtaining an observed set of sample values. For vibration based damage detection problems, acceleration data are typically measured

through sensors. To experimentally characterize the underlying probabilistic distribution model for measured acceleration data, the acceleration response of a laboratory truss bridge structure subjected to broad-band white noise was measured at a sampling rate of 5 kHz. A total of 100,000 acceleration data were measured. According to a statistical analysis of the measured acceleration data in the form of a histogram (See Fig. 2), the random process turns out to follow the Gaussian process. As shown in Fig. 3, the normal probability plot indicates that the acceleration data follow the normal distribution. If the plot is linear with $R^2 \approx 1$ as shown in Fig. 3, the random data come from the normal process.

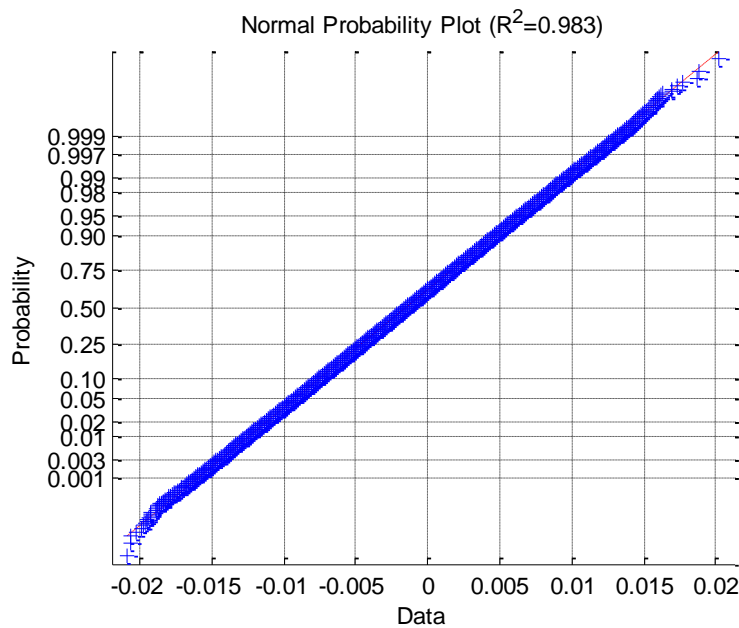


Fig. 3 Normal probability paper plot for the raw acceleration data measured from a laboratory structure subjected to broad-band white noise (500 mV amplitude)

Therefore, the likelihood function is based on the normal distribution. Assuming a normal distribution for a random variable X, a general form of the likelihood function with a set of sampled data x_i ($i=1, \dots, n$) is expressed as

$$Lik(x_1, x_2 \dots x_n : \mu, \sigma^2) = \prod_{i=1}^n f(x_i : \mu, \sigma^2) = \prod_{i=1}^n \frac{1}{\sigma\sqrt{2\pi}} \exp\left(-\frac{(x_i - \mu)^2}{2\sigma^2}\right) \quad (10)$$

where μ and σ denote the sample mean and standard deviation of the sampled data, respectively. In this paper, DSIs are suggested based on the log likelihood ratio of wavelet packet coefficients from the selected frequency bands. Therefore, through the same statistical analyses, probabilistic distributions of the wavelet packet coefficients are investigated.

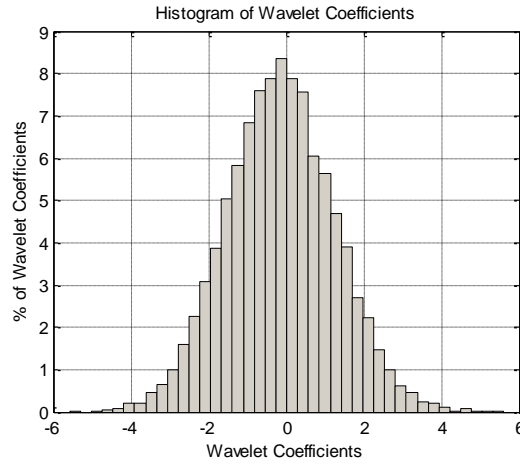


Fig. 4 Histogram of wavelet coefficients in the wavelet packet of time domain data measured from a laboratory structure subjected to broad-band white noise (500 mV amplitude)

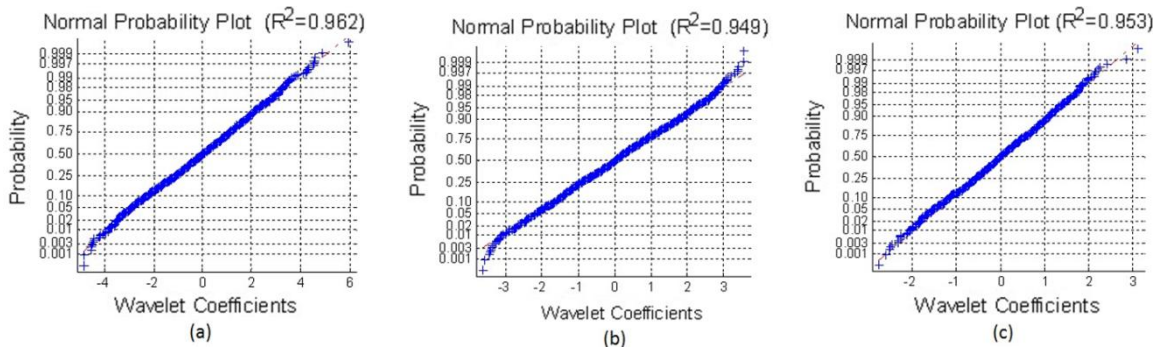


Fig. 5 Normal probability paper plots for the wavelet packets of time-domain acceleration data: the level of decomposition= 6 and selected (a) wavelet packet C_6^1 , (b) wavelet packet C_6^2 and (c) wavelet packet C_6^3

As shown in Figs. 4 and 5, it was experimentally proven that all the wavelet packet coefficients also follow the normal distribution. This means that the WPD is a linear transformation of time-domain random signals (Chendeb *et al.* 2006). It is worth noting that acceleration response of civil structures such as a building under vehicle traffic loading and a tower under wind gust may not show normal distributions. In this case, through the goodness-of-fit test, corresponding probability distribution function has to be determined first as demonstrated in this section and used in calculating the likelihood function.

In this paper, log likelihood functions of the wavelet packet coefficients ($C_{j,k}^i$) were used instead of the likelihood function for two indispensable reasons: 1) computing log likelihood functions is more computationally efficient than the likelihood functions and 2) likelihood functions in terms of the wavelet packet coefficients produce numerical instability due to huge numbers. By taking a natural logarithm of the likelihood function, the log likelihood function is expressed as

$$\begin{aligned} \text{Ln Lik}(C_{j,1}^i, \dots, C_{j,n}^i : \mu, \sigma^2) &= \ln \left[\prod_{k=1}^n \frac{1}{\sigma_c \sqrt{2\pi}} \exp \left(-\frac{(C_{j,k}^i - \mu_c)^2}{2\sigma_c^2} \right) \right] \\ &= n \ln \left(\frac{1}{\sigma_c \sqrt{2\pi}} \right) - \sum_{k=1}^n \left[\frac{(C_{j,k}^i - \mu_c)^2}{2\sigma_c^2} \right] = -n \ln \sigma_c - \frac{n}{2} \ln(2\pi) - \sum_{k=1}^n \left[\frac{(C_{j,k}^i - \mu_c)^2}{2\sigma_c^2} \right] \end{aligned} \quad (11)$$

where n indicates the number of coefficients in the selected wavelet packet component. n is identical to $N/2^j$ where N is the total number of the original time domain data. μ_c and σ_c indicate the sample mean and sample standard deviation of the wavelet packet coefficients, respectively. As shown in Eq. (11) taking the natural logarithm will change arithmetic operators from multiplications to additions. The likelihood ratios are usually used for the likelihood ratio test (LRT) that is a statistical test of the goodness-of-fit between two probabilistic models based on the observed time series data (Hald 1999, Mood *et al.* 1974). In terms of the log likelihood function in Eq. (11), the log likelihood ratio is expressed as

$$\text{Ln LR}(C_j^i | C_j^{i'}) = \frac{\text{Ln Lik}(C_{j,1}^i, C_{j,2}^i, \dots, C_{j,n}^i : \mu_c, \sigma_c^2)}{\text{Ln Lik}(C_{j,1}^{i'}, C_{j,2}^{i'}, \dots, C_{j,n}^{i'} : \mu_c', \sigma_c'^2)} \quad (12)$$

where $C_{j,n}^i$ and $C_{j,n}^{i'}$ denote two coefficient sets of the WPD at j th frequency scale of the raw time domain data from two different locations. For the log likelihood ratio computation, i and j are determined at a specific modulation and level of decomposition based on the following selection procedures proposed in this paper.

Selection of Wavelet Packet and Level of Decomposition: In application of wavelet packets to damage detection problems, proper selection of wavelet packets should be performed. In this paper, based on the sensitivity of the log likelihood ratio to changes in damage level and magnitude of the log likelihood ratio, a method for selecting the most proper wavelet packet was proposed. Considering multi-resolution characteristics of wavelet packets, resolutions of both time and frequency domains are determined by the number of time-domain samples and the level of decomposition. Therefore, the level of decomposition should be determined so that fundamental natural frequencies are separated into each wavelet packet. It is suggested to choose the wavelet packet of the frequency band that includes natural frequencies corresponding to fundamental modes. It is postulated that fundamental modes are more influenced by component damage than higher modes.

2.3 Computational efficiency of the DSI for real-time damage identification

As previously mentioned, the log likelihood ratio is adopted for computational efficiency since multiplication is known to require more computation time than additions. Fig. 6 shows a comparison of the computation times required for the likelihood ratio and for the log likelihood ratio with WPD based on the acceleration data from two channels. The computation speed of log likelihood ratio is shown to be 3.5 to 4 times faster than that of likelihood ratio.

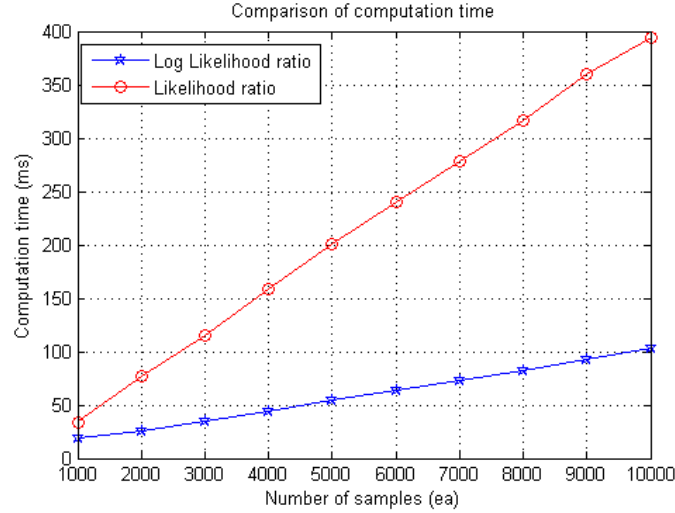


Fig. 6 Comparison of computation times required for the likelihood and log likelihood ratio

Typically, the log likelihood of the wavelet coefficients from a damaged location is smaller than the log likelihood of the wavelet coefficients from an undamaged location, since damage has a reducing effect of the energy of signals. Therefore the log likelihood ratio can be used as a DSI. The log likelihood ratio is a statistical index to be used as the DSI for real-time reference-free damage detection in this paper. A detailed feature extraction process for the reference-free schemes will be explained in the following section.

2.4 Statistical reference-free damage identification algorithm

Reference-free damage detection has a practical advantage in cases where baseline signals are not available. Most in-built bridge structures do not provide baseline signals from pristine structural conditions. Without relying on the baseline signals, the log likelihood ratio of coefficients of the selected wavelet packets between two different locations allows us to detect damage.

Following the definition in Eq. (12), a simpler notation for the log likelihood ratio is introduced as

$$\text{Ln LR}(C_k^\alpha | C_k^\beta) \equiv \text{LogLikelihoodRatio between location } \alpha \text{ and } \beta \quad (13)$$

where α and β denote the location of sensors over the structure and k denotes the x, y, z direction of the original signal. C_k^α and C_k^β are wavelet coefficients in the selected wavelet packet. According to multiple experimental tests and observations, the log likelihood from a damaged location tends to become smaller than that from an undamaged location. Explaining such observations based on physical perspectives, the level of disorder in the signals increases as the level of damage increases. Thus, it results in distraction of the inherent probabilistic distribution of wavelet coefficients from normal process. If there are p sensor locations and the raw acceleration

data are measured in x, y and z directions at each of p locations, the statistical reference-free DSI for the location β is defined as

$$DSI_k^\beta = \sum_{\alpha=1}^p \text{Ln LR}_k(C_k^\alpha | C_k^\beta), \quad k = x, y, z \quad (14)$$

For each sensor location, the statistical DSI is defined as a sum of the ratios of the log likelihood values at all sensor locations to the log likelihood at the current sensor location. The p DSIs are expanded as shown in Table 1. If damage occurred at a location d , the log likelihood value of the wavelet coefficients from the damaged location is smaller than that from other undamaged locations. Therefore, the log likelihood ratios between undamaged locations and the damaged location- $\text{Ln LR}_k(C_k^1 | C_k^d)$, $\text{Ln LR}_k(C_k^2 | C_k^d)$... $\text{Ln LR}_k(C_k^p | C_k^d)$ that are highlighted in the Table 1- will show relatively higher values than the other log likelihood ratios except $\text{Ln LR}(C_k^d | C_k^d)$ that corresponds to one.

Table 1 Computation of statistical reference-free DSI at p sensor locations

DSI_k^1	$\text{Ln LR}_k(C_k^1 C_k^1) + \text{Ln LR}_k(C_k^2 C_k^1) + \dots + \text{Ln LR}_k(C_k^{p-1} C_k^1) + \text{Ln LR}_k(C_k^p C_k^1)$
DSI_k^2	$\text{Ln LR}_k(C_k^1 C_k^2) + \text{Ln LR}_k(C_k^2 C_k^2) + \dots + \text{Ln LR}_k(C_k^{p-1} C_k^2) + \text{Ln LR}_k(C_k^p C_k^2)$
...	...
DSI_k^d	$\text{Ln LR}_k(C_k^1 C_k^d) + \text{Ln LR}_k(C_k^2 C_k^d) + \dots + \text{Ln LR}_k(C_k^{p-1} C_k^d) + \text{Ln LR}_k(C_k^p C_k^d)$
...	...
DSI_k^p	$\text{Ln LR}_k(C_k^1 C_k^p) + \text{Ln LR}_k(C_k^2 C_k^p) + \dots + \text{Ln LR}_k(C_k^{p-1} C_k^p) + \text{Ln LR}_k(C_k^p C_k^p)$

Based on this procedure, p statistical reference-free DSIs can be calculated and any sensor location showing a larger DSI than a threshold value will be identified as a damaged location.

Determination of Threshold Value: After reference-free DSIs are computed, those DSIs are compared with a threshold value. Factors associated with the threshold value include the number of channels (S), the number of coefficients in the selected wavelet packet (C), and the type of test structure. Typically, the log likelihood ratio value between two wavelet packets from undamaged locations is close to one when the number of wavelet coefficients in the selected wavelet packet (C) is sufficiently large enough to reveal its statistical normal distribution. In such a case, the log likelihood ratio will become close to one. Therefore, the minimum threshold value can be set to S when the number of wavelet coefficients in the selected wavelet packet (C) is sufficiently large enough to show a normal distribution. When the number of C decreases, the value of the log likelihood ratio can be greater than one because the number of realizations is not sufficient to reveal the normal distribution. Furthermore, the threshold values can vary depending on the type

of structures. Because there is no clear criterion to set the threshold value, it is based on the test experiences. When statistical reference-free DSIs exceed the threshold value, the damage detection system generates warning alarms at the corresponding damaged locations.

3. Damage identification procedures and implimentation

In this section, detailed procedures of statistical reference-free real-time damage identification are summarized for practical implementation. The damage detection procedures are implemented in a remote front panel using national instruments (NI)-LabVIEW virtual instrumentation (VI) program.

3.1 Procedures of statistical reference-free real-time damage identification

Fig. 7 depicts the schematic procedures of statistical reference-free real-time damage identification as three steps.

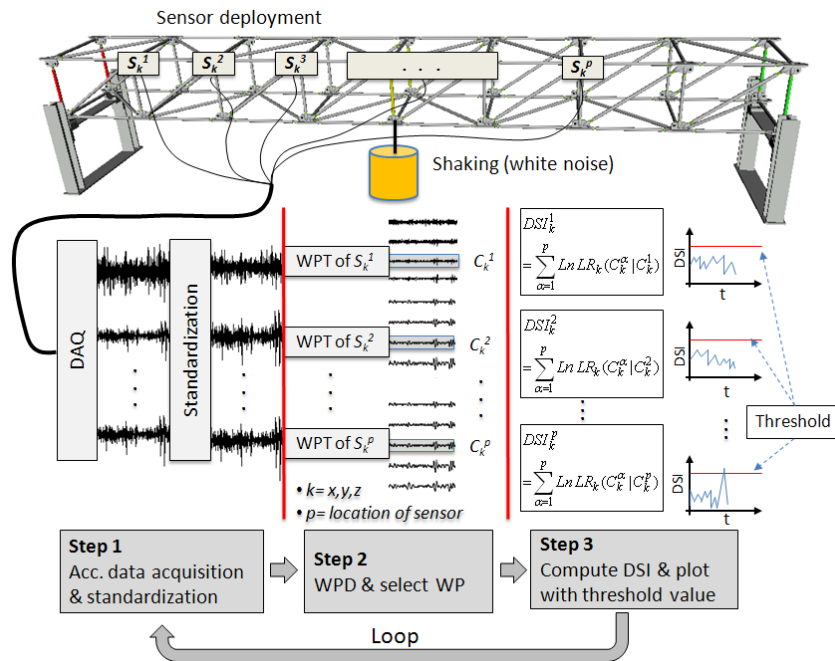


Fig. 7 Schematic procedures for the proposed real-time damage detection algorithm

Step 1 Data Acquisition and Standardization: The first step of the damage detection procedure is acquiring time-domain acceleration signals from sensors deployed on the structure. The acceleration data are acquired at a user-defined sampling rate. The number of sampled data in

a window is also determined by users. Prior to the WPD, a standardization process is applied to the acceleration signals in order to obtain all signals with zero sample mean and unit variance. Through this process, different amplitudes of signals at various locations due to any possible signal shift can be scaled and shifted to have zero-means, keeping frequency contents and probabilistic distribution information of the original raw signals.

$$x_i = \frac{X_i - \mu}{\sigma}, \quad \mu = \frac{\sum_{i=1}^n X_i}{n}, \quad \sigma = \sqrt{\frac{\sum_{i=1}^n (X_i - \mu)^2}{n}} \quad (15)$$

In Eq (15), X_i denotes the original time domain signal and x_i denotes the standardized signal. μ and σ denote the mean and standard deviation of the original acceleration signals.

Step 2 Selection of Wavelet Packet and Level of Decomposition: All the standardized signals are decomposed using WPD based on the selected mother wavelet and frequency scale. In this paper, one wavelet packet showing the largest magnitude and the highest sensitivity of the log likelihood to the damage level is chosen. For the selection of frequency scale, the frequency band of the selected wavelet packet should include the fundamental frequency for its higher damage sensitivity. Considering the frequency band of the wavelet packet, the sixth frequency scale in WPD was tested in this paper.

Step 3 Computation of Statistical DSIs: Once each wavelet packet is selected from different locations, the sample mean (μ_c) and variance (σ_c^2) of the wavelet coefficients are computed for use in calculations of the log likelihood ratios. Statistical reference-free DSIs are computed based on the sum of log likelihood ratios at different sensor locations as explained in Eq. (14) and Table 1. The computed statistical DSIs at each sensor location are compared with a predetermined threshold value; if a DSI is greater than the threshold value, it will provide an alarm to inspectors.

Step 4 Computation of DSIs for Next Window: Finally, all of the three steps are repeated in a loop as shown in Fig. 7 .

3.2 Implementation of statistical real-time reference-free damage detection system

In the remote front panel, users can specify input parameters such as the sampling rate, the number of time domain samples in a window, the mother wavelet, the level of wavelet decomposition, notational path for the selected wavelet packet, and channel for viewing the coefficients of a selected channel. Users can also specify the threshold level. When statistical DSIs exceed the threshold value, an alarm light will be turned on so that users can visually notice the damaged location in a real-time mode. In this paper, the threshold value is set to three to seven times of the number of channel (S). All of the 24 damage indices (eight DSIs for each of the three directions) were graphically presented on the remote front panel and the graphical plots are updated every second with the damage indices calculated based on the Eq. (14).

4. Experimental verifications of damage identification with a laboratory-size truss

In this section, a laboratory-size truss bridge structure is introduced and the entire experimental test set-up based on the structure is described. Using the test set-up, different damage scenarios

such as bolt loss, member fracture and bolt loosening were tested for verifying the proposed real-time reference-free damage detection algorithm.

4.1 Laboratory truss bridge structure

A laboratory-size truss bridge structure was designed and manufactured for SHM research. The structure with a dimension of Length \times Width \times Height = 4.8 m \times 0.56 m \times 0.42 m is an 8-bay, 4.8 meters (184 inch) span truss bridge constructed of steel pipes and steel connections with simply-supported boundary conditions. The structure was assembled using 100 steel pipes; 200 clevises; 36 T-joints; and 200 bolts, 200 nuts, and 136 washers. Two washers were used between clevis and the vertical web of the T-joints in order to fill the gap between clevis and the web. The geometric configuration of the truss bridge structure is shown in Fig. 8.

Thick-walled steel seamless pipes (ASTM A106 grade) with the same sectional properties but in five different lengths are used as shown in Fig. 9(a). One end has a left-hand thread and the other end has a right-hand thread. These opposing threads provide significant flexibility to adjust the length of the members during the assembly process, thus ensuring ease and accuracy (to the design drawings) of the final assembled structure shape.

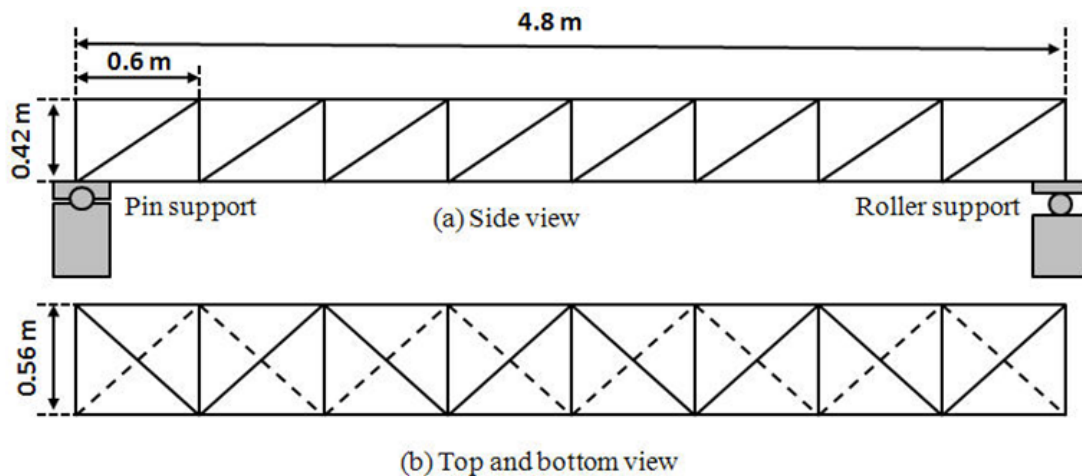


Fig. 8 Design of T-Joint component

A connection system capable of providing the strength to carry the loads and flexibility to simulate several damage cases is designed. Specifically, the connection has the following features: 1) ability to connect up to eight steel members at any joint; 2) convenient assembly and disassembly for rapid testing of various damage scenarios; 3) efficient fabrication; 4) ability to accommodate sensors. A total of 36 connections are utilized throughout the structure, and a typical connection is shown in Fig. 9 (b).

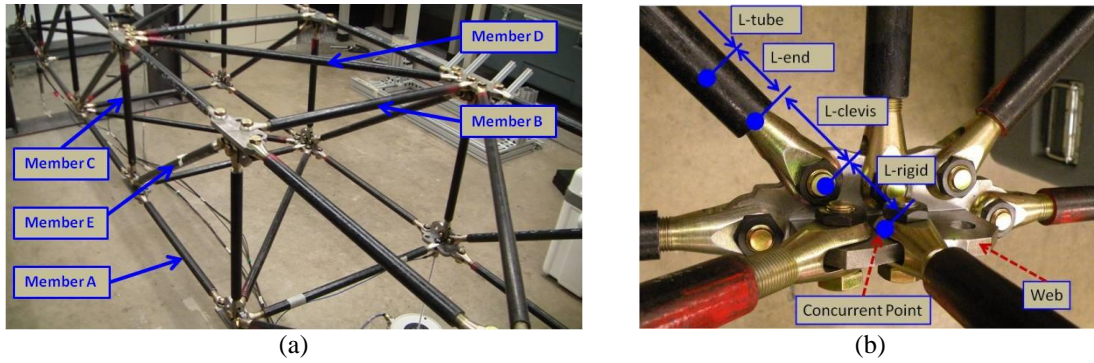


Fig. 9 (a) Five types of load carrying members of the laboratory-size truss bridge structure and (b) T-joint with 7 joining members



Fig. 10 Boundary condition of the truss bridge structure (a) roller support and (b) hinge support

The truss bridge structure is supported by rollers at one end and hinges at the other. Those supports are similar to ones used in real-life bridge structures as shown in Fig. 10. More details on the truss bridge structure can be found in (Shang *et al.* 2010).

4.2 Experimental test setup and damage scenarios

Eight triaxial accelerometers (Dytran 3093B1) were instrumented on the truss bridge structure for measuring accelerations. An electrodynamic shaker (LDS V408) was used to shake the structure. An amplifier and a power supply were used to operate the shaker. A function generator (Agilent 33250A) was also used to generate excitation signals. A data acquisition system consisting of three NI 4472B dynamic signal acquisition moduls (each provides eight channels) and a NI PXI 8105 controller within NI-PXI-1402 chassis provides 24 channels from which acceleration data are measured. The test setup was configured to measure structural vibration response of the truss bridge structure with different types of damage under broad-band white noise excitations. Fig. 11 shows joint identification (ID) numbers to distinguish damaged locations. To shake the structure in Z direction, the LDS V408 shaker is attached at joint ID 22.

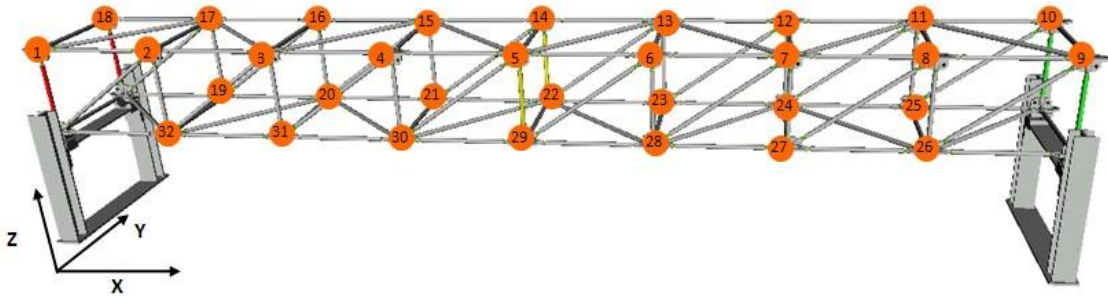


Fig. 11 Joint ID of the truss bridge structure

In truss bridge structures, various kinds of damage such as loss of bolts, bolt loosening, reduction of member stiffness due to sectional loss, cracks, material deterioration, fracture, or combinations of them are frequently observed. Therefore, in this paper, three different damage types are tested: a) loss of bolts b) section loss of a member, and c) loosening of bolts as shown in Fig. 12.

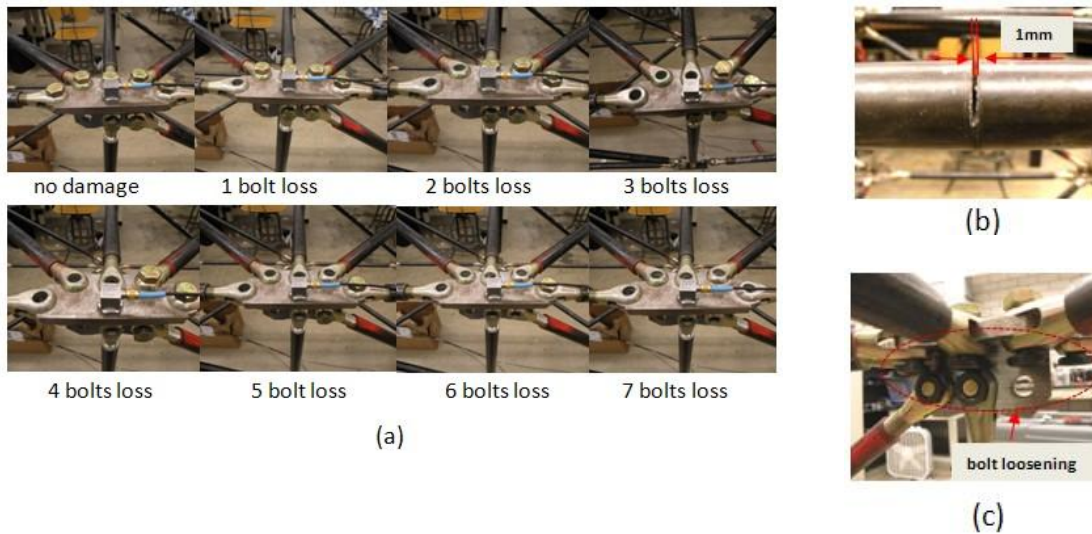


Fig. 12 Three damage types (a) loss of bolts, (b) section loss of member and (c) loosening of bolts

As shown in Fig. 12 (a), seven damage scenarios with loss of bolts were made by removing bolts one-by-one at joint ID 16. As shown in Fig. 12(b), 50% section loss of a member 1 (joint ID 15-16) was made with 1 mm thickness saw-cut at the center of the member. As shown in Fig. 12(c), all of the bolts are loosened at the selected damaged joint. First damage type (loss of bolts) is intended to select a wavelet packet to be used for computing the proposed statistical DSIs. As

proposed in Section 2.2, the sensitivity of the proposed statistical DSI to the damage and its magnitude are considered for wavelet packet selection. To evaluate the proposed statistical DSIs under multiple damaged locations, loosening of bolts at different locations were tested. As such, different damage types and damage scenarios were created and summarized in Table 2 with the joint ID numbers.

Table 2 Damage scenarios with different types of damage

Damage Type	Damage Level	Damaged Position	Sensor Position
a. Bolt Loss	1 bolt loss	16	16
	2 bolts loss	16	16
	3 bolts loss	16	16
	4 bolts loss	16	16
	5 bolts loss	16	16
	6 bolts loss	16	16
	7 bolts loss	16	16
b. Sectional loss	Sensor deployment 1	center of member 1(15-16)	member 1(15-16), member 2(16-17) member 3(2-3), member 4(3-4)
	Sensor deployment 2	center of member 1(15-16)	member 1(15-16), member 2(5-14) member 3(11-12), member 4 (28-7)
c. Bolt Loosening	single damage	JDS1 12	10,11,12, 13, 15, 16, 17, 18
	double damage	JDS2 17	10,11,12, 13, 15, 16, 17, 18
	triple damage	JDS3 11,14	10,11,12, 13, 15, 16, 17, 18
	single damage	JDS4 16,26	11,23,16,19,26,6,3,32
	double damage	JDS5 6,20,3	12,24,14,20,8,6,3,32
	triple damage	JDS6 24,17,3	24,13,27,6,21,17,30,3

In this paper, broad-band white noise signals were used to excite the structure. Loading intensity for each test was arbitrarily set within a range from 400 mV to 520 mV. Due to the mandatory standardization process, the proposed method is immune to variability of loading amplitudes. The presented tests proved that the proposed method can identify damage locations as long as the loading intensity is sufficient to induce structural vibration. We also tested the proposed method under sweep sine excitation signals. However, because broad-band white noise signals are more similar to in-field ambient excitations, the sweep sine signals were not used.

4.3 Sensitivity test for selecting wavelet packet

In this section, the sensitivity of the proposed statistical DSIs was tested by varying the level of joint damage in order to select a wavelet packet to be used for the DSI. From the joint ID 16, the acceleration signals (10,000 data) sampled at 5 kHz sampling rate were standardized and then decomposed by WPD to the sixth level of decomposition. All the selected parameters used for computing the DSI are summarized in the Table 3.

Table 3 Parameter set for bolt loss damage scenarios

Damage Type	Sampling Rate (Hz)	Number of Samples	Mother Wavelet	Level	Path for Selected Wavelet Packet	Frequency Range (Hz)
Bolt Loss	5,000	10,000	db2	6	000000(1 st Packet)	0- 39.06
					000001(2 nd packet)	39.06-78.12
					000010(3 rd packet)	78.12-117.18

Seven statistical DSIs were computed by using selected wavelet packets from an undamaged state and seven damaged states that range from loss of one bolt to losses of seven bolts at joint ID 16. To perform statistical sensitivity analyses, ten windows of time-domain acceleration data were used to obtain ten sets of the first, second and third wavelet packets and the averaged log likelihood ratios for the first three wavelet packets were plotted with error bars as shown in Fig. 13.

The results clearly showed that the DSIs based on the first wavelet packet have higher magnitude and sensitivity to the damage than the DSIs based on the second and third wavelet packets. It is because the frequency range (0- 39.06 Hz) of the first wavelet packet includes first three fundamental frequencies (14.45 Hz, 20.98 Hz and 29.73 Hz) identified by the frequency domain decomposition (FDD) analysis. Therefore, it is important to identify the fundamental frequencies of test structures for guiding selection of a wavelet packet and determine the level of decomposition so that the selected wavelet packet includes the damage sensitive fundamental natural frequencies.

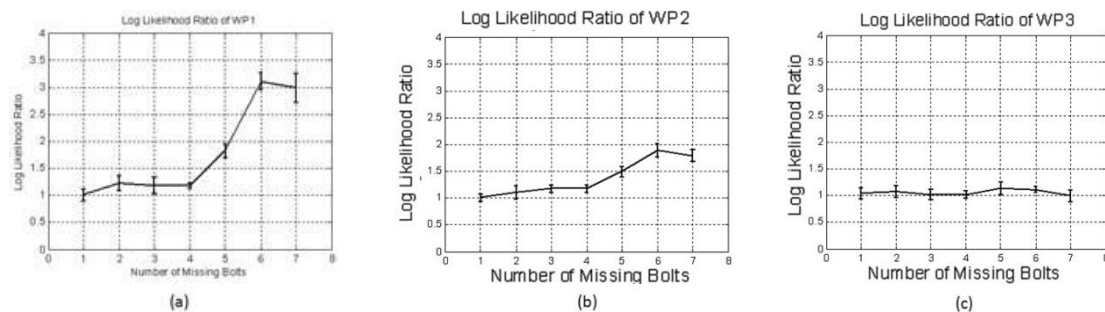


Fig. 13 Change of log likelihood ratio versus the number of missing bolts at Joint 16: (a) test results of WP1(C^1_6), (b) test results of WP2(C^2_6) and (c) test results of WP3 (C^3_6)

4.4 Experimental test results: identification of member damage

In this section, detecting member damage by the proposed DSIs was demonstrated with two different sensor deployments. Due to the limited number of sensors, two specific sensor deployments were tested as shown in the Figs. 14(a) and 14(b). As shown in Fig. 14(c), two sensors were attached per each of the selected members in order to measure relative accelerations.

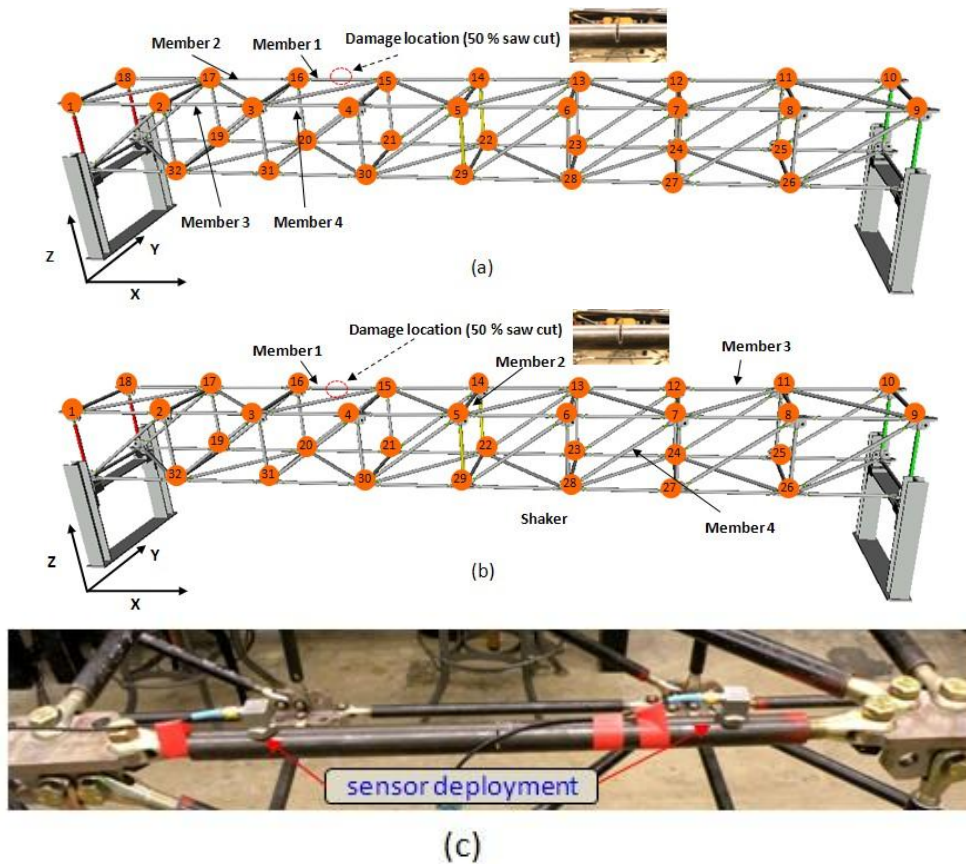


Fig. 14 Test configuration for identifying a member with sectional loss (50% saw-cut) (a) sensor deployment 1, (b) sensor deployment 2 and (c) installation of sensors on the member

Table 4 Parameter set for sectional loss damage detection

Damage Type	Sampling Rate(Hz)	Number of Samples	Mother Wavelet	Level	Path for Selected Wavelet Packet	Frequency Range (Hz)
Sectional loss (50% saw-cut)	5000Hz	10000	db2	6	000000 (1 st Packet)	0- 39.06

Fig. 14(a) shows that three top chord members (Member 2(joint ID 16-17), Member 3(joint ID 2-3) and Member 4(joint ID 3-4)) adjacent to the damaged member are selected. Fig. 14(b) shows the second sensor deployment in which two top chord members (Member 1(joint ID 15-16)) and Member 3(joint ID 11-12)) in X direction, one transverse member (Member 2(joint ID 5-14)) in Y direction, and one diagonal member (Member 4(joint ID 28-7)) placed on the X-Z plane are selected. In the second sensor deployment, the selected members are located far distance from each other and their axial directions are set to be different. Time-domain acceleration data (10000 samples) were sampled at 5-kHz sampling rate. First, the measured accelerations were standardized by Eq. (15). For computations of the DSIs, relative accelerations were computed simply by subtracting acceleration data measured at one end from those measured at the other end per each member. Four relative acceleration signals were decomposed by WPD to the sixth scale with db2 mother wavelet. Based on the results of the sensitivity test presented in Section 4.3, the first packet was selected to compute the DSIs because frequency range of the selected wavelet packet includes fundamental frequencies as explained in Section 4.3. Detailed information on the parameters selected for the computation of DSIs is summarized in Table 4.

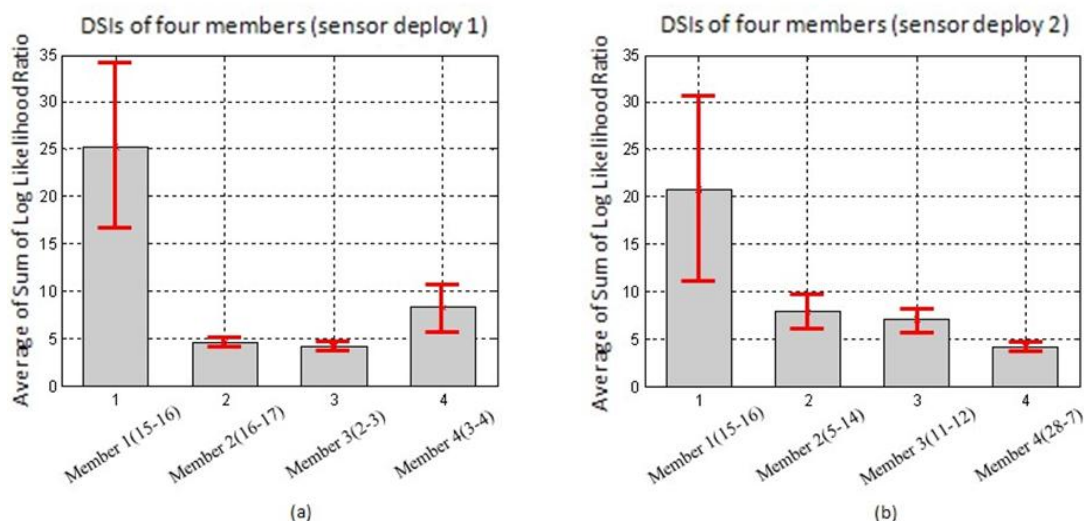


Fig. 15 Results of member damage identification (a) test results of sectional loss with sensor deployment 1 and (b) test results of sectional loss with sensor deployment 2

The tests were repeated up to 30 times in order to perform statistical analyses of the DSIs and accordingly computed DSIs were averaged and plotted with error bars as shown in Fig. 15. The test results with two different sensor deployments show that the proposed method could successfully locate the damaged member (Member 1(joint ID 15-16)). According to the test results, the DSIs computed from tests with members having the same length and axial directions showed better performance than those computed from tests using members with different lengths and axial directions. Although we could monitor only four members due to a limited number of sensors, the damage specificity is expected to increase as more sensors are available.

4.5 Experimental test results: identification of joint damage

For detecting joint damage made by loosening bolts, the remote front panel of the statistical reference-free real-time damage detection system developed in the NI-LabVIEW VI program was used. The proposed statistical reference-free DSI was experimentally verified by detecting the damaged joints. All the information of parameters, selected wavelet packet and corresponding frequency ranges of the wavelet packet were summarized in Table 5. Joint damage scenario (JDS) 1, 3 and 4 were tested with 5 kHz sampling rate, 5000 samples in a window, db2 for mother wavelet, sixth level of decomposition and wavelet packet (000000) that includes the frequency band from 0 Hz to 39.06 Hz. JDS 2, 5 and 6 were tested with 2 kHz sampling rate, 2000 samples in a window, db2 for mother wavelet, sixth level and wavelet packet (000001) that includes the frequency band from 16.13 Hz to 32.25 Hz. As shown in Table 5, all of the selected wavelet packets include natural frequencies of the truss bridge structure.

Table 5 Parameter sets for joint damage scenarios

Damage Scenario	Sampling Rate(Hz)	Number of Samples(ea) in a Window	Mother Wavelet	Level	Path for		
					Selected Wavelet Packet	Threshold Value	Frequency Range (Hz)
JDS1	5 kHz	5000	db2	6	000000	50	0- 39.06
JDS2	2 kHz	2000	db2	6	000001	50	16.13- 32.25
JDS3	5 kHz	5000	db2	6	000000	50	0- 39.06
JDS4	5 kHz	5000	db2	6	000000	50	0- 39.06
JDS5	2 kHz	2000	db2	6	000001	50	16.13- 32.25
JDS6	2 kHz	2000	db2	6	000001	50	16.13- 32.25

Log likelihood ratios are updated in nearly real-time mode on the remote front panel for all of the tested JDSs as shown in Fig. 16 through Fig. 21. In both of the single joint damage cases, the locations of damage could clearly be detected with the damage alarm light. Compared to other undamaged joints, the statistical DSIs from joint ID 12 and 17 fluctuated very much, with noticeably large amplitudes. It indicates damage at joint ID 12 and 17. It was also observed that the DSIs in X and Y direction were more effective in detecting joint damage than the DSI in Z direction. Figs. 18 and 19 show monitoring states on the remote front panel in the case of double joint damage scenarios. Similarly, the proposed DSIs from the damaged joints exceeded the preset threshold value and indicated damage. Like the single damage case, the DSIs in Z direction were relatively smaller than those in X and Y direction. Figs. 20 and 21 show monitoring states on the remote front panel for the cases of triple joint damage. With an equivalent level of specificity, all three damaged joints were successfully detected with the proposed statistical DSI. Due to relatively small energy level in Z direction, DSIs in Z direction were smaller than those in other

directions. As a result, all the single and multiple damaged locations were clearly detected by the statistical reference-free real-time damage detection algorithm. Although it was not included in this paper, the proposed reference-free DSIs showed consistency and repeatability in detecting locations of damaged joints. Therefore, the proposed statistical DSI is expected to be very useful for monitoring structural health of in-field truss bridge structures in real-time mode because of its robustness, high specificity to damage, reference-free feature and fast analysis times.

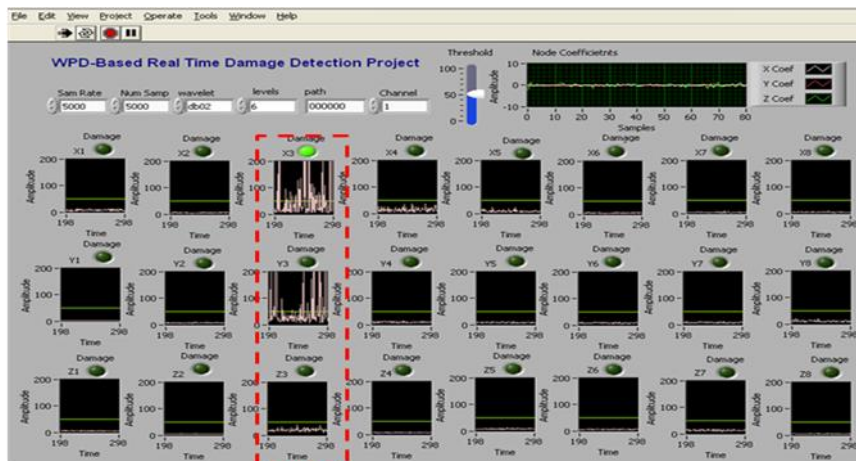


Fig. 16 Result of joint damage scenario 1(damaged location at joint ID 12)

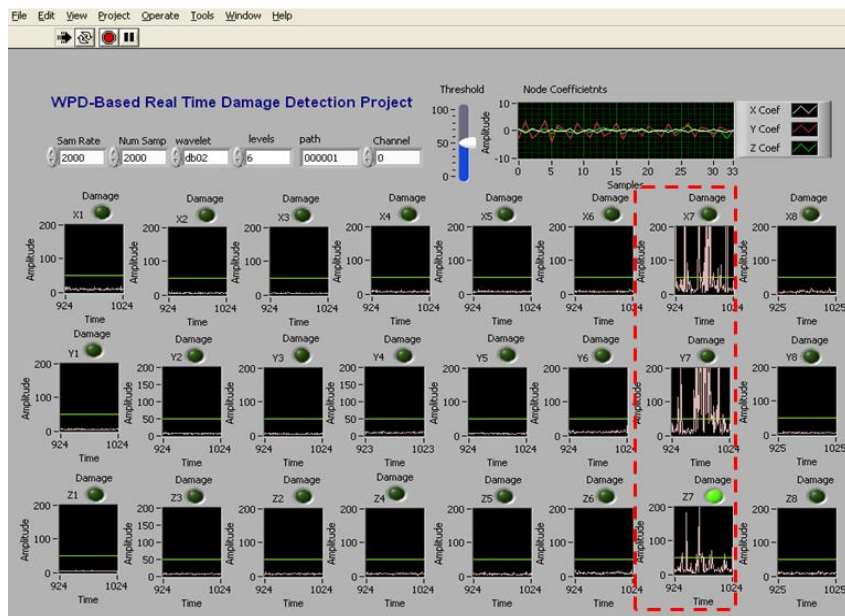


Fig. 17 Result of joint damage scenario 2 (damaged location at joint ID 17)

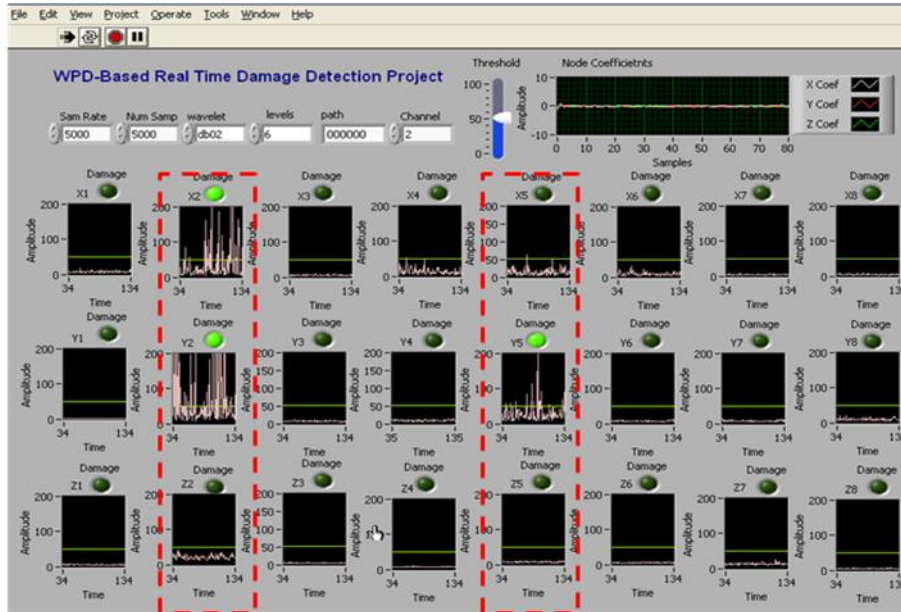


Fig. 18 Result of joint damage scenario 3 (damaged location at joint ID 11,14)

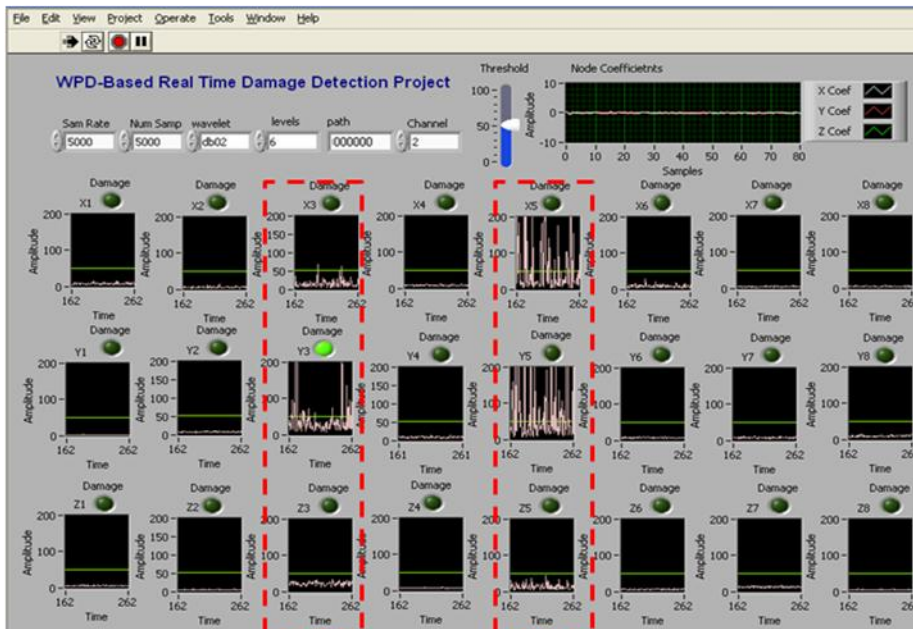


Fig. 19 Result of joint damage scenario 4 (damaged location at joint ID 16 and 26)

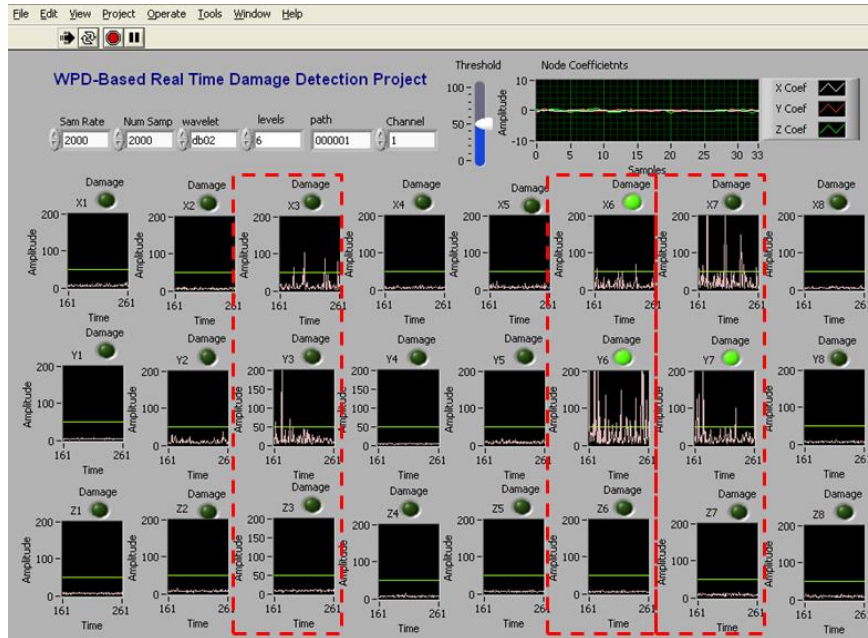


Fig. 20 Result of joint damage scenario 5 (damaged location at joint ID 6, 20 and 3)

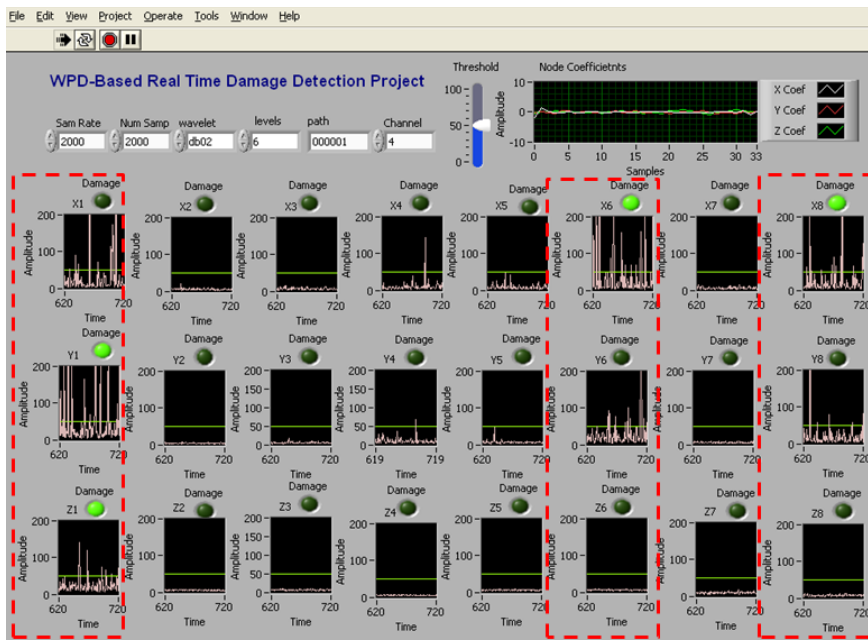


Fig. 21 Result of joint damage scenario 6 (damaged location at joint ID 24, 17 and 3)

However, since the DSIs proposed in this paper are sensitive to the selection of wavelet packet, the frequency range of the selected wavelet packets should include the fundamental frequencies in order to successfully detect the damaged locations.

5. Conclusions

In this paper, a statistical reference-free damage detection method was proposed for real-time monitoring of truss bridge structures. In particular, the proposed method does not need vibration signals from undamaged structures because of its effective pairing methodology of signals from different locations at the current damaged state. Therefore, the proposed damage detection method can be applied to damaged bridge structures without referencing signals from the undamaged structure. From this point of view, the proposed damage detection method is considered more effective than other damage detection methods that need reference data from undamaged state because the monitored data from initial pristine structures are not always available. Moreover, it was demonstrated that signal processing and analyses in terms of the log likelihood ratio was much faster than computations in terms of the likelihood ratio. Therefore, the proposed damage detection method can monitor bridge structures continuously in the real-time mode. This potentially helps public users by providing more time for evacuation in order to prevent a catastrophic disaster.

The proposed statistical damage detection method is based on WPD of vibration signals and log likelihood ratio for their statistical signal analyses. For this purpose, it was postulated that probabilistic distributions of vibration signals from damaged and undamaged locations are very different, and this difference can be used for the purpose of damage detection. Log likelihood ratios were computed based on the normal distribution model because both time-domain acceleration signals and wavelet coefficients showed the normal distribution from the demonstrated tests. The proposed method was verified by using a laboratory-size truss bridge structure in detecting various types of damage that are frequently observed in real-life structures – such as loss of bolts, member stiffness reduction by sectional loss, and damaged joints caused by bolt loosening. Since it is important to select the wavelet packet that is the most sensitive to damage, a sensitivity test was conducted and a procedure for selecting the wavelet packet was proposed in this paper. According to various experimental demonstrations and verifications, the proposed damage detection method was proven to be very effective in detecting various types of damage without reference data from undamaged structures. Especially for the damage detection of joint damage by bolt loosening, a statistical reference-free real-time damage detection system was developed by using NI-LabVIEW and was applied to the experimental verification. Through this system, all of the damaged joint locations were successfully located without any false alarm, even with damage at multiple joints. The proposed statistical reference-free real-time damage detection system can also be useful to monitor any abnormality caused by sensor failures.

Acknowledgements

This research is supported by the New Faculty Startup Fund from the University of Akron. The authors are grateful for their support.

References

- Aktan, A.E., Grimmelman, K., Ciloglu, K. and Pan, Q. (2004), "Evaluating the reliability of highway bridges following hazards in real-time by structural health monitoring (RT-SHM-D+P)", *Nondestruct. Det. Measure. Homeland Security II*, **5395**, 111-121.
- Aldrich, J. (1997), "R. A. Fisher and the making of maximum likelihood 1912-1922", *Stat. Sci.*, **12**(3), 162-176.
- Amiri, G.G. and Asadi, A. (2009), "Comparison of different methods of wavelet and wavelet packet transform in processing ground motion records", *Int. J. Civil Eng.*, **7**(4), 248-257.
- Chang, C.C. and Sun, Z. (2005), "Structural damage localization using spatial wavelet packet signature", *Smart Struct. Syst.*, **1**(1), 29-46.
- Chendeb, M., Khalil, M. and Duchene, J. (2006), "Methodology of wavelet packet selection for event detection", *Signal Process.*, **86**(12), 3826-3841.
- Coifman, R.R. and Wickerhauser, M.V. (1992), "Entropy-Based Algorithms for Best Basis Selection", *IEEE T. Inform. Theory*, **38**(2), 713-718.
- Daubechies, I. (1992), *Ten Lectures on Wavelets*, Philadelphia, PA: Society for Industrial and applied Mathematics.
- Ding, Y.L. and Li, A.Q. (2007), "Structural health monitoring of long-span suspension bridges using wavelet packet analysis", *Earthq. Eng. Eng. Vib.* **6**(3), 289-294.
- Grabowska, J., Palacz, M. and Krawczuk, M. (2008), "Damage identification by wavelet analysis", *Mech. Syst. Signal Pr.*, **22**(7), 1623-1635.
- Hald, A. (1999), "On the history of maximum likelihood in relation to inverse probability and least squares", *Stat. Sci.*, **14**(2), 214-222.
- Han, J.G., Ren, W.X. and Sun, Z.S. (2005), "Wavelet packet based damage identification of beam structures", *Int. J. Solids Struct.*, **42**(26), 6610-6627.
- Hu, C.S. and Afzal, M.T. (2006), "A wavelet analysis-based approach for damage localization in wood beams", *J. Wood Sci.*, **52**(5), 456-460.
- Jiang, X. and Adeli, H. (2007), "Pseudospectra, MUSIC, and dynamic wavelet neural network for damage detection of highrise buildings", *Int. J. Numer. Meth. Eng.*, **71**(5), 606-629.
- Jiang, X.M. and Mahadevan, S. (2008), "Bayesian wavelet methodology for structural damage detection", *Struct. Health Monit.*, **15**(7), 974-991.
- Jiang, X.M., Mahadevan, S. and Adeli, H. (2007), "Bayesian wavelet packet denoising for structural system identification", *Struct. Health Monit.*, **14**(2), 333-356.
- Kim, S.B. and Sohn, H. (2007), "Instantaneous reference-free crack detection based on polarization characteristics of piezoelectric materials", *Smart Mater. Struct.*, **16**(6), 2375-2387.
- Liew, K.M. and Wang, Q. (1998), "Application of wavelet theory for crack identification in structures", *J. Eng. Mech. -ASCE*, **124**(2), 152-157.
- Masri, S.F., Sheng, L.H., Caffrey, J.P., Nigbor, R.L., Wahbeh, M. and Abdel-Ghaffar, A.M. (2004), "Application of a web-enabled real-time structural health monitoring system for civil infrastructure systems", *Smart Mater. Struct.*, **13**(6), 1269-1283.
- Mood, A.M., Graybill, F.A. and Boes, D.C. (1974), *Introduction to the theory of statistics*, McGraw-Hill Series in Probability and Statistics, 410.
- Newland, D.E. (1993), *Random vibrations, spectral and wavelet analysis 3rd Ed.*, Harlow and John Wiley: New York.
- Ni, Y.Q., Zhou, X.T. and Ko, J.M. (2006), "Experimental investigation of seismic damage identification using PCA-compressed frequency response functions and neural networks", *J. Sound Vib.*, **290**(1-2), 242-263.
- Nigbor, R.L. and Diehl, J.G. (1997), "Two years' experience using OASIS real-time remote condition monitoring system on two large bridges", *Struct. Health Monit.*, 410-417.

- Ovanesova, A. and Suarez, L.E. (2004), "Applications of wavelet transforms to damage detection in frame structures", *Eng. Struct.*, **26**(1), 39-49.
- Shang, S., Yun, G.J., Lee, S.G., Caicedo, J.M. and Narasimhan, S. (2010), "Development of a benchmark laboratory structure for finite element model updating", *Proceedings of the 5th International Conference on Bridge Maintenance, Safety and Management*. Philadelphia, PA.
- Shinde, A. and Hou, Z.K. (2005), "A wavelet packet based sifting process and its application for structural health monitoring", *Struct. Health Monit.*, **4**(2), 153-170.
- Sun, Z. and Chang, C.C. (2002), "Structural damage assessment based on wavelet packet transform", *J. Struct. Eng.-ASCE*, **128**(10), 1354-1361.
- Sun, Z. and Chang, C.C. (2007), "Vibration based structural health monitoring: wavelet packet transform based solution", *Struct. Infrastruct. E.*, **3**(4), 313-323.
- Taha, M.M.R., Noureldin, A., Lucero, J.L. and Baca, T.J. (2006), "Wavelet transform for structural health monitoring: A compendium of uses and features", *Struct. Health Monit.*, **5**(3), 267-295.
- Tsai, C.S., Hsieh, C.T. and Huang, S.J. (2006), "Enhancement of damage-detection of wind turbine blades via CWT-based approaches", *IEEE T. Energy Convers.*, **21**(3), 776-781.
- Wang, W.J. and McFadden, P.D. (1996), "Application of wavelets to gearbox vibration signals for fault detection", *J. Sound Vib.*, **192**(5), 927-939.
- Yen, G.G. and Lin, K.C. (2000), "Wavelet packet feature extraction for vibration monitoring", *IEEE T. Ind. Electron.*, **47**(3), 650-667.
- Yun, G.J. (2010), *Collaboratory Website*. <http://isehm.mech.uakron.edu:8084/Benchmark> .
- Yun, G.J., Lee, S.G., Carletta, J. and Nagayama, T. (2011), "Decentralized damage identification using wavelet signal analysis embedded on wireless smart sensors", *Eng. Struct.*, **33**, 2162-2172.
- Zhou, Z.J., Hu, C.H., Han, X.X. and Chen, G.J. (2005), "Adaptive wavelet packet neural network based fault diagnosis for missile's amplifier", *Adv. Neural Networks - Isnn 2005, Pt 3, Proceedings*, **3498**, 591-596.